HHS Public Access

Author manuscript

Science. Author manuscript; available in PMC 2020 March 08.

Published in final edited form as:

Science. 2019 March 08; 363(6431): 1093–1097. doi:10.1126/science.aau6313.

Stoichiometry controls activity of phase separated clusters of actin signaling proteins

Lindsay B. Case[1,2], **Xu Zhang**[1,2], **Jonathon A. Ditlev**[1,2], **Michael K. Rosen**[1,2,*]

[1]The HHMI Summer Institute, Marine Biological Laboratory, Woods Hole, MA 02543, USA.

[2]Department of Biophysics and Howard Hughes Medical Institute, University of Texas Southwestern Medical Center, Dallas, TX 75390, USA.

Abstract

Biomolecular condensates concentrate macromolecules into foci without a surrounding membrane. Many condensates appear to form through multivalent interactions that drive liquid-liquid phase separation (LLPS). LLPS increases the specific activity of actin regulatory proteins toward actin assembly by the Arp2/3 complex. We show that this occurs because LLPS of the Nephrin/Nck/N-WASP signaling pathway on lipid bilayers increases membrane dwell time of N-WASP and Arp2/3 complex, consequently increasing actin assembly. Dwell time varies with relative stoichiometry of the signaling proteins in the phase separated clusters, rendering N-WASP and Arp2/3 activity stoichiometry-dependent. This mechanism of controlling protein activity is enabled by the stoichiometrically-undefined nature of biomolecular condensates. Such regulation should be general among signaling systems that assemble through multivalent interactions and drive non-equilibrium outputs.

One sentence summary

Phase separation increases activity of signaling proteins by lengthening their membrane dwell times in a stoichiometry dependent fashion.

Biomolecular condensates are two- and three-dimensional compartments in eukaryotic cells that concentrate specific collections of proteins and nucleic acids without an encapsulating membrane (1, 2). Many condensates behave as dynamic liquids, and are believed to form through liquid-liquid phase separation (LLPS) driven by interactions between multivalent constituents (1–3). Unlike macromolecular machines such as the ribosome, which have discrete subunit stoichiometries and size, condensates can form with a wide range of component stoichiometries, and range in size from hundreds to thousands of nanometers. While the mechanisms that promote and regulate LLPS *in vitro* and in cells are increasingly well understood, the biochemical functions that arise from organization of macromolecules into these meso-scale assemblies remain largely unknown. In particular, it is unknown

*Corresponding author: michael.rosen@utsouthwestern.edu (M.K.R.).

Author contributions: L.B.C., J.A.D. and X.Z. prepared reagents. L.B.C. performed the experiments and analyzed data. L.B.C. and M.K.R. wrote the manuscript. All authors commented on the manuscript.

Competing interests: The authors declare no conflicts of interest.

Data and materials availability: All data required to reproduce and extend these results are available in the Dryad Digital Repository.

whether condensates function primarily as concentrating devices or whether their physical properties also frequently alter specific activities of the collection of resident molecules (analogous to specific activity in enzymology but applied here to the condensate as a whole).

We have described two analogous signaling systems that form membrane-associated condensates *in vitro* and in cells (4–6). These control actin assembly in podocyte cells of the kidney and in activated T cells, respectively. Both pathways are initiated by transmembrane proteins, Nephrin and Linker for Activation of T cells (LAT), respectively, whose disordered cytoplasmic tails are phosphorylated on multiple tyrosine residues in response to upstream stimuli. These phospho-proteins then interact with collections of adaptor proteins containing SH2 domains, SH3 domains and proline-rich motifs (PRMs). Multivalency in these molecules enables their assembly and concomitant phase separation, forming micron-scale signaling clusters on supported lipid bilayers (SLBs) *in vitro* and at the plasma membrane of cells.

In both systems, clusters assemble actin filaments through the adaptor protein Nck, its ligand N-WASP, and the actin nucleation factor, the Arp2/3 complex. In the LAT system, we previously showed that LLPS increases the specific activity of molecules in the pathway toward activating the Arp2/3 complex (5). However, without knowing the mechanism, it was impossible to know whether this effect is specific to actin assembly or might be more general to other signaling systems. Here we sought to understand the mechanism by which LLPS causes this increase in activity, how this mechanism could be exploited to regulate signaling output, and whether such effects might be observed in other signaling systems.

We attached fluorescently labeled His_8-Nephrin phosphorylated on its three tyrosine residues (his-pNephrin) at a density of ~1000 molecules/μm^2 on SLBs containing 2% Ni-NTA lipids. His-pNephrin alone is diffuse on SLBs, but upon addition of Nck and a constitutively active Alexa488 labeled N-WASP (N-WASP hereafter, Fig. S1a) the proteins undergo LLPS to form micron sized clusters (Fig. S1b–d). To initiate actin polymerization, we added 1 μM actin (5% Alexa647 labeled), 3 nM Arp2/3 complex, and 6 nM capping protein (CapZ), the latter to focus the assay on actin nucleation rather than filament elongation (Figs. 1a–b, S2a). This led to robust actin polymerization in the plane of the SLB, as observed by total internal reflection fluorescence (TIRF) microscopy (Fig. S2a–c). We quantified actin polymerization inside and outside of the clusters through measuring Alexa647-actin fluorescence intensity over time (Fig. 1c). Inside clusters, actin fluorescence increased rapidly and plateaued within 2 minutes. Outside clusters, actin fluorescence increased more slowly. The actin assembly rate at half-maximal intensity (red lines, Fig. 1c) was ~6-fold faster inside clusters than outside. To separate the effects of increased N-WASP concentration within clusters from effects on specific activity of the clusters, we divided the rates by the local N-WASP intensity (Fig. 1d). This N-WASP-normalized actin assembly rate was ~3-fold faster inside than outside of clusters. Outside clusters, the normalized assembly rate was comparable to a negative control lacking the Arp2/3 complex. When this background is subtracted, the N-WASP-normalized actin assembly rate inside the clusters was ~14-fold higher than outside. Thus, in addition to being at higher density, the specific activity of N-WASP is substantially increased inside phase separated clusters, analogous to our previous observations with LAT signaling clusters (5).

The Arp2/3 complex is divalent, and binds N-WASP with 1:2 stoichiometry (7, 8). This could lead to non-linear recruitment and activity of the Arp2/3 complex with N-WASP density (9). However, as detailed in Supplemental Figure 3, the amount of Alexa647-labeled Arp2/3 complex recruited to the SLB scaled linearly with his-N-WASP density, and the N-WASP-normalized actin assembly rate was not density dependent. Thus, higher density is unlikely to account for the increased specific activity of clusters.

Huang et al. have shown with single-molecule analysis that increased membrane dwell time induced by phase separation enhances activity in slow, multi-step signaling cascades that are driven out of equilibrium by irreversible steps (10, 11). Actin nucleation by the Arp2/3 complex is a multi-step process that initiates with binding of an Arp2/3:$WASP_2$:$actin_2$ assembly (Arp2/3 assembly hereafter) to an existing “mother” actin filament. A series of incompletely understood conformational changes of the Arp2/3 complex and mother filament (12, 13) then lead to dissociation of WASP proteins, irreversible attachment of Arp2/3 complex to the mother filament and initiation of daughter filament growth (14). Single molecule studies and kinetic modeling have shown that this process is slow, and WASP-bound intermediates have lifetimes in the 0.5–10 second range (14–16). Since nucleation by the Arp2/3 complex is a slow, multi-step process that involves at least one irreversible step we hypothesized that membrane dwell time might be a key parameter affecting N-WASP specific activity.

To measure N-WASP membrane dwell time we fused the photoactivatable fluorophore, mEos2 to its N-terminus and measured the fluorescence decrease over time after photoactivation (which is due to dissociation from the membrane, Fig. S4). We found that N-WASP membrane dwell time increased from 18 sec outside clusters to 30 sec inside clusters (Fig. 1e). Thus, LLPS increases the membrane dwell time of N-WASP in nephrin clusters.

We used several different approaches to experimentally perturb dwell time and examined the corresponding effects on activity. First, we quantitatively compared his-N-WASP attached directly to SLBs to an identical density of N-WASP attached indirectly to the bilayer through his-Nck (Fig. 2a). The average dwell time of the former is > 2 hours (Fig. S5), while that of the latter is < 20 s (Fig 2b). The N-WASP-normalized actin assembly rate of stably attached his-N-WASP was more than 40 times that of his-Nck + N-WASP (Fig. 2c). Membrane dwell time can also be increased by increasing the local density of binding sites, likely through a combination of decreased rate of dissociation from binding partners and also more rapid membrane rebinding after initial dissociation (17). We engineered his-Nck analogues with either three repeats (his-Nck$(SH3)_3$) or six repeats (his-Nck$(SH3)_6$) of the second SH3 domain (Fig. S6a). To prevent phase separation of his-Nck$(SH3)_6$ we added 300 mM NaCl to the buffer (Fig. S6b). Doubling the local density of SH3 domains increased N-WASP membrane dwell time from 7.9 sec to 9.5 sec (Fig. S6c) and increased the N-WASP normalized actin assembly rate 2.2-fold (Fig. S6d). Finally, we clustered his-Nck$(SH3)_6$ with pNephrin (Fig. 2d), increasing N-WASP membrane dwell time from 9.5 sec to 12.1 sec (Fig. 2e) and the N-WASP-normalized actin assembly rate 3-fold (Fig. 2f). Thus, increasing N-WASP membrane dwell time through three independent molecular mechanisms consistently increased the N-WASP-normalized actin assembly rate.

Next, we sought to systematically alter the membrane dwell time of N-WASP within clusters. We reasoned that dwell time is likely related to the number of SH3-PRM interactions that connect each N-WASP to Nck molecules that are also bound to pNephrin ("N-WASP connectivity"). This connectivity should, in turn, be dictated by the relative stoichiometry of his-pNephrin, Nck and N-WASP. To test this idea initially we used SpringSaLaD (18) to simulate pNephrin-Nck-N-WASP clustering on membranes (Fig. S7a–d). We found that N-WASP connectivity shows a non-monotonic dependence on Nck concentration when pNephrin density and N-WASP concentration are held constant (Fig. 3a). At low concentrations most Nck is bound to pNephrin, and increasing Nck increases multivalent SH3-PRM interactions to N-WASP, thus increasing N-WASP connectivity. But once Nck molecules exceed Nephrin pTyr sites, further increases in Nck decrease connectivity since N-WASP molecules become decorated with Nck molecules that are not bound to pNephrin (Fig. 3b, Fig. S8).

To test this model experimentally, we varied stoichiometry in nephrin clusters by keeping the membrane density of his-pNephrin constant (~1,000 molecules/μm^2), and varying the concentrations of N-WASP and Nck in solution (Fig S9a–c). For three N-WASP conditions (100 nM N-WASP, 250 nM N-WASP, and maintaining a constant 1:2 N-WASP:Nck ratio), we varied Nck concentration from 100 nM to 2 μM. In all titrations, the membrane dwell time of N-WASP showed a similar non-monotonic relationship with Nck concentration, with a maximum at 200–500 nM Nck (Fig. 3c).

Since the Arp2/3 complex is the proximal nucleator of actin filaments, we also examined its membrane dwell time under these conditions. Using a mask generated from the image of N-WASP (Fig. 3d), we tracked single Alexa647-Arp2/3 complex particles inside and outside of clusters. Particles that remained on the membrane for at least 3 s were classified as long-lived. Outside clusters only 6% of particles were long-lived (Fig 3e), while inside clusters 21% were long-lived (Fig. 3e). Photobleaching occurred at a much slower rate than particle dissociation from the membrane, and does not appreciably affect these values ($k_{dissoc,\ outside}$ = 1.67 s^{-1}, $k_{dissoc,\ inside}$ = 0.35s^{-1}, k_{bleach} = 0.023 s^{-1}, Figure S10a). In titration experiments, the percent of long-lived Arp2/3 complex had the same non-monotonic dependence on Nck concentration (Fig. 3f) and positively correlated with the N-WASP dwell time (Pearson r = 0.63, $p<0.01$, Fig. 3g). This correlation suggests that within clusters the Arp2/3 complex often dissociates from the membrane in complex with N-WASP. In contrast, the percent of long-lived Arp2/3 complexes outside clusters is insensitive to stoichiometry and never exceeds 7% (Fig. S10b).

To test whether stoichiometric control of dwell time regulates the rate of actin assembly, we performed actin assembly assays across the same Nephrin/Nck/N-WASP stoichiometries as in Figures 3C and F. The N-WASP-normalized actin assembly rate was non-monotonic with Nck concentration (Fig. 4a), and strongly correlated with N-WASP membrane dwell time among all the data (Pearson r = 0.85, $p<0.0001$, Fig. 4b). This normalized rate did not positively correlate with N-WASP density (Fig. S12a). It showed only a weak correlation with N-WASP density divided by N-WASP solution concentration (Fig. S12c), which would be expected to correlate with binding affinity of N-WASP for the clusters, suggesting that dissociation rate rather than binding affinity governs the actin assembly rate. A similar

correlation with N-WASP dwell time, but not density or binding affinity, was found when actin assembly rates were normalized to the density of Arp2/3 complex (Fig. 4c, Pearson r=0.82, p<0.0002, Figs. S11, S12b, S12d), suggesting that the long-lived N-WASP-Arp2/3 assemblies are the active species at clusters. In cellular experiments, we observed a similar non-monotonic dependence of both N-WASP dwell time (Fig. 3h–j) and N-WASP-normalized actin assembly (Figs. 4d–f, Fig. S13) on the density of Nck at nephrin clusters on the plasma membrane, and N-WASP dwell time positively correlated with actin assembly (Fig 4g, Pearson r = 0.73, p<0.02). Thus, relative stoichiometry is sufficient to regulate specific activity of clusters containing full-length N-WASP in the complex cellular environment. Because the progression from the initial assembly of Arp2/3:$WASP_2$:$actin_2$ plus mother filament to the commencement of daughter filament growth is not understood mechanistically, we are not able to develop a rigorous kinetic model to explain our data. Nevertheless, the data clearly show that stoichiometry controls specific activity in phase separated Nephrin clusters.

In summary, we found that phase separation of pNephrin, Nck and N-WASP on SLBs increases the specific activity of clusters by increasing the membrane dwell time of N-WASP and its assemblies with the Arp2/3 complex, consequently increasing Arp2/3-dependent actin assembly. Additionally, since the relative stoichiometry of the components dictates dwell time, the activity of the pathway is controlled by stoichiometry. These observations suggest that phase separation may enable a binary switch between low-activity and high-activity states of this pathway, and that variations in stoichiometry may enable fine-tuning of the response within the high-activity regime. Together, phase separation and stoichiometric control could help suppress noise in low-activity states, but still allow modulation after a commitment to action has been made. These mechanisms may contribute to the observed Nck density-dependence of actin polymerization in cells (19) and could regulate diverse actin signaling pathways that utilize phase separation at membranes (5, 20, 21). Since the multivalent SH2-pTyr and SH3-PRM interactions that promote LLPS in this system, as well as the slow, multi-step, non-equilibrium downstream process, are found in numerous signaling pathways, these behaviors should be generalizable. Consistent with this idea, the LAT-Grb2-SOS pathway also phase separates and shows dwell time-dependent activation of Ras (11). Stoichiometry-dependent control of specific activity is distinct from canonical mechanisms of allostery and co-localization. This mechanism requires biomolecular assemblies (not necessarily phase separated) that can form across a range of component stoichiometries, unlike molecular machines. Our data support the idea that material/physical properties, determined by the dynamic behaviors of component molecules, may be generally important in defining the biochemical activities of biomolecular condensates (1, 2).

Supplementary Material

Refer to Web version on PubMed Central for supplementary material.

Acknowledgements

We thank Ethan Garner (Harvard) for suggesting addition of CapZ to the assays to focus quantification on actin nucleation rather than filament elongation, Les Loew (Uconn Health) for helpful advice about the SpringSaLaD software, and Jay Groves and William Huang for discussions on dwell time and technical advice.

Funding: L.B.C. is a Robert Black Fellow of the Damon Runyon Cancer Research Foundation (DRG-2249-16). This work was supported by a grant from the Welch Foundation (I-1544 to M.K.R.), a National Research Service Award from NIDDK (F32 DK101188 to J.A.D.), and a Howard Hughes Medical Institute Collaborative Innovation Award.

References and Notes

1. Banani SF, Lee HO, Hyman AA, Rosen MK, Biomolecular condensates: organizers of cellular biochemistry. Nat. Rev. Mol. Cell Biol 18, 285–298 (2017). [PubMed: 28225081]
2. Shin Y, Brangwynne CP, Liquid phase condensation in cell physiology and disease. Science. 357, eaaf4382 (2017). DOI: 10.1126/science.aaf4382 [PubMed: 28935776]
3. Li P et al., Phase transitions in the assembly of multivalent signalling proteins. Nature. 483, 336–340 (2012). [PubMed: 22398450]
4. Banjade S, Rosen MK, Phase transitions of multivalent proteins can promote clustering of membrane receptors. Elife. 3, e04123 (2014).
5. Su X et al., Phase separation of signaling molecules promotes T cell receptor signal transduction. Science. 352, 595–599 (2016). [PubMed: 27056844]
6. Kim MK, Kalappurakki S, Mayor JM, Rosen S, Multivalent interactions generated membrane receptor clusters that move through actomyosin contraction. In Preperation.
7. Padrick SB et al., Hierarchical regulation of WASP/WAVE proteins. Mol. Cell 32, 426–38 (2008). [PubMed: 18995840]
8. Padrick SB, Doolittle LK, Brautigam CA, King DS, Rosen MK, Arp2/3 complex is bound and activated by two WASP proteins. Proc. Natl. Acad. Sci. U. S. A 108, E472–9 (2011). [PubMed: 21676863]
9. Yang T, Baryshnikova OK, Mao H, Holden MA, Cremer PS, Investigations of bivalent antibody binding on fluid-supported phospholipid membranes: the effect of hapten density. J. Am. Chem. Soc 125, 4779–84 (2003). [PubMed: 12696896]
10. Huang WYC et al., Phosphotyrosine-mediated LAT assembly on membranes drives kinetic bifurcation in recruitment dynamics of the Ras activator SOS. Proc. Natl. Acad. Sci. U. S. A 113, 8218–23 (2016). [PubMed: 27370798]
11. Huang JT, Alvarez WYC, Kondo S, Lee Y, Chung YK, Lam JK, Kuriyan HYM, Groves J, "A molecular assembly phase transition and kinetic proofreading modulate Ras activation by SOS."
12. Rodnick-Smith M, Liu S-L, Balzer CJ, Luan Q, Nolen BJ, Identification of an ATP-controlled allosteric switch that controls actin filament nucleation by Arp2/3 complex. Nat. Commun 7, 12226 (2016). [PubMed: 27417392]
13. Espinoza-Sanchez S, Metskas LA, Chou SZ, Rhoades E, Pollard TD, Conformational changes in Arp2/3 complex induced by ATP, WASp-VCA, and actin filaments. Proc. Natl. Acad. Sci 115, E8642–E8651 (2018). [PubMed: 30150414]
14. Smith B. a. et al., Three-color single molecule imaging shows WASP detachment from Arp2/3 complex triggers actin filament branch formation. Elife. 2013, 1–25 (2013).
15. Zalevsky J, Lempert L, Kranitz H, Mullins RD, Different WASP family proteins stimulate different Arp2/3 complex-dependent actin-nucleating activities. Curr. Biol 11, 1903–1913 (2001). [PubMed: 11747816]
16. Smith BA, Daugherty-Clarke K, Goode BL, Gelles J, Pathway of actin filament branch formation by Arp2/3 complex revealed by single-molecule imaging. Proc. Natl. Acad. Sci. U. S. A 110, 1285–90 (2013). [PubMed: 23292935]
17. Oh D et al., Fast rebinding increases dwell time of Src homology 2 (SH2)-containing proteins near the plasma membrane. Proc. Natl. Acad. Sci 109, 14024–14029 (2012). [PubMed: 22886086]
18. Michalski PJ, Loew LM, SpringSaLaD: A Spatial, Particle-Based Biochemical Simulation Platform with Excluded Volume. Biophys. J 110, 523–529 (2016). [PubMed: 26840718]
19. Ditlev JA et al., Stoichiometry of Nck-dependent actin polymerization in living cells. J. Cell Biol 197, 643–658 (2012). [PubMed: 22613834]
20. Sun Y et al., Switch-like Arp2/3 activation upon WASP and WIP recruitment to an apparent threshold level by multivalent linker proteins in vivo. Elife. 6, 652 (2017).

21. Castello A et al., Nck-mediated recruitment of BCAP to the BCR regulates the PI(3)K-Akt pathway in B cells. Nat. Immunol 14, 966–975 (2013). [PubMed: 23913047]

22. Cooper JA, Pollard TD. Methods to measure actin polymerization. Methods Enzymol 85, 182–210 (1982). [PubMed: 6889668]

23. Doolittle LK, Rosen MK, Padrick SB. Purification of native Arp2/3 complex from bovine thymus. Methods Mol Biol. 1046, 231–50 (2013). [PubMed: 23868592]

24. Hansen SD, Zuchero JB, Mullins RD. Cytoplasmic Actin: Purification and Single Molecule Assembly Assays. Methods Mol Biol. 1046:145–70. (2013). [PubMed: 23868587]

25. Banjade S et al., Conserved interdomain linker promotes phase separation of the multivalent adaptor protein Nck. Proc. Natl. Acad. Sci. U. S. A 112, E6426–35 (2015). [PubMed: 26553976]

26. Picco A, Mund M, Ries J, Nédélec F, Kaksonen M, Visualizing the functional architecture of the endocytic machinery. Elife. 4, e04535 (2015).

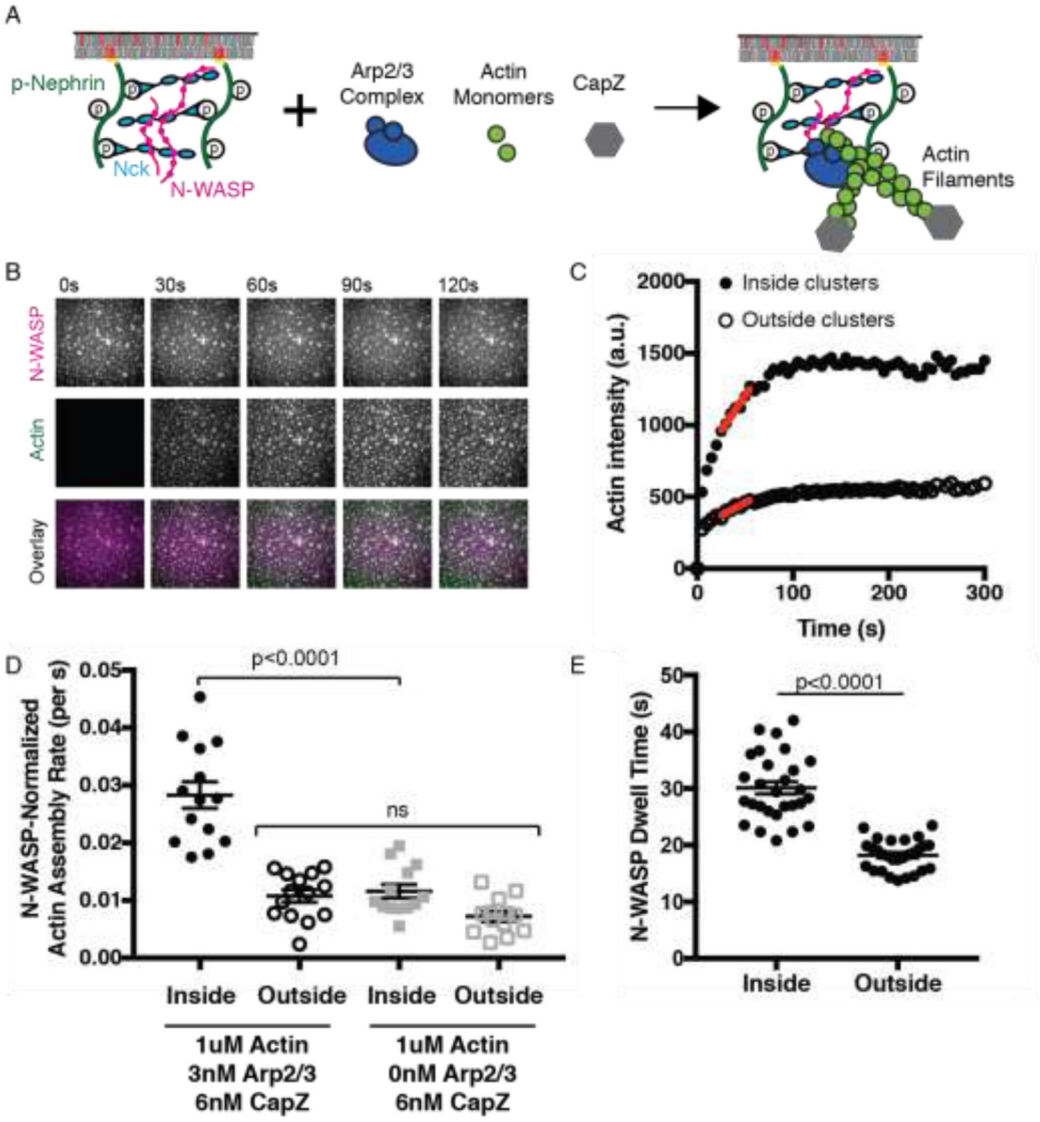

Fig. 1.

The specific activity of N-WASP is increased in phase separated membrane clusters. **(A)** Schematic of actin assembly assay. Molecules not drawn to scale. **(B)** Total Internal Reflection Fluorescence Microscopy (TIRF) images of N-WASP (top) and Actin (middle) during actin polymerization. Clusters were formed by adding N-WASP (1μM, 15% Alexa488 labeled) and Nck (2μM) to membrane-bound pNephrin (~1000 molecules/μm^2). Actin (1 μM, 5% Alexa647 labeled), Arp2/3 complex (3 nM), and CapZ (6 nM) were added at t = 0 s. Scale bar, 5 μm. **(C)** Quantification of mean actin intensity inside and outside of clusters from images in (a). Red line indicates rate at half-maximal intensity. **(D)** Quantification of N-WASP-normalized actin assembly rate from 14 measurements containing Arp2/3 complex and 13 measurements without Arp2/3 complex. In these experiments, N-WASP is enriched ~2.2-fold inside clusters. Significance tested with one-way ANOVA followed by post hoc Tukey test. **(E)** Quantification of mEos2-N-WASP membrane dwell time inside and outside of clusters from n=28 measurements. Significance

tested with an unpaired t-test. In D and E, points represent individual measurements, horizontal line represents mean, and error bars represent SEM.

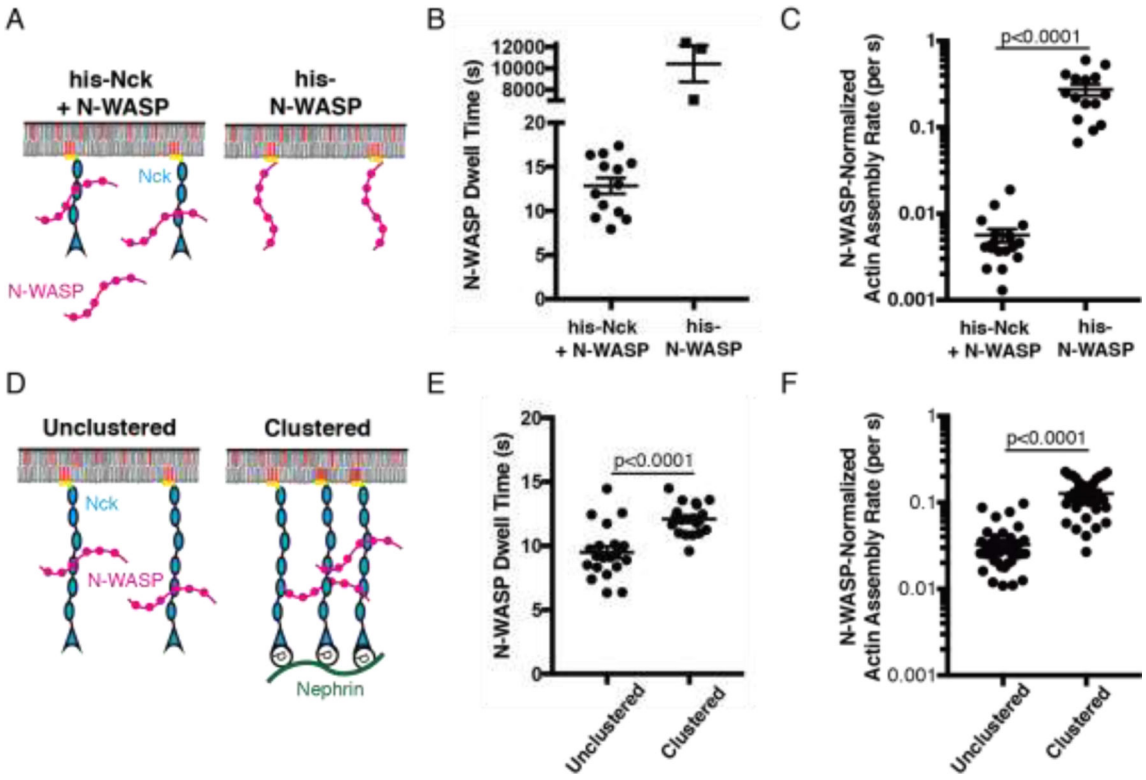

Fig. 2.

Increasing N-WASP membrane dwell-time is sufficient to increase its specific activity. **(A)** Schematic of experimental setup in B-C. Molecules not drawn to scale. **(B)** Dwell time of mEos2-N-WASP (n=13) and his-N-WASP-Alexa488 (n=3), the latter as described in Figure S5. **(C)** N-WASP-normalized actin assembly rate for his-N-WASP (n=15) and his-Nck + N-WASP (n=18). **(D)** Schematic of experimental setup in E-F. Molecules not drawn to scale. **(E)** Dwell time of mEos2-N-WASP unclustered (n=20) and clustered (n=20). **(F)** N-WASP-normalized actin assembly rate of unclustered (n=40) and clustered (n=32) N-WASP. In all graphs, points represent individual measurements, horizontal line represents mean, error bars represent SEM, significance tested with unpaired t test. Note that data in Figures 2e-f and S6c–d are not directly comparable to those in Figure 4, as different buffer and actin concentrations were used in the different experiments. Both datasets are, however, internally comparable.

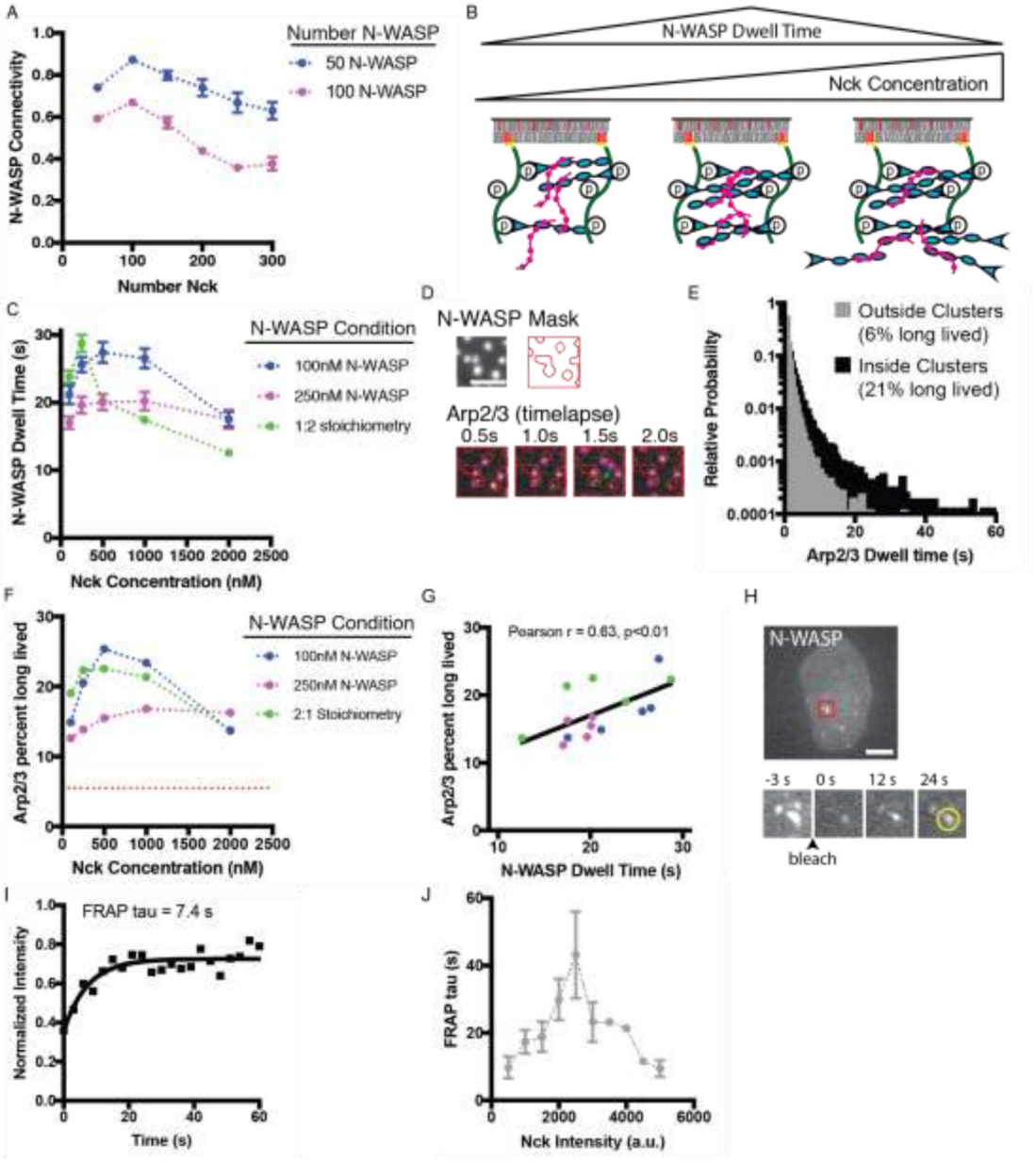

Fig. 3.

Stoichiometry regulates membrane dwell time of N-WASP and Arp2/3 complex in phase separated membrane clusters.

(A) N-WASP connectivity in computational simulations. The number of pNephrin (25 molecules) and N-WASP (50 or 100; blue and magenta, respectively) molecules was kept constant and the number of Nck molecules was varied. Data points represent the mean +/− SEM from six simulations. **(B)** Summary of simulation predictions. Molecules not drawn to scale. **(C)** Experimental measurement of mEos2-N-WASP membrane dwell time. Clusters were formed by adding N-WASP (15% mEos2 labeled) and Nck at the indicated concentrations to membrane-bound pNephrin (~1000 molecules/μm^2). Data points represent mean +/− SEM from at least 13 measurements. Details about number of measurements are

in Table S2 **(D)** Representative Total Internal Reflection Fluorescence Microscopy (TIRF) images from a single particle tracking experiment. Clusters were formed by adding N-WASP (1μM, 15% Alexa488 labeled) and Nck (2 μM) to membrane-bound pNephrin (~1000 molecules/μm^2). Arp2/3 complex (3 nM unlabeled, 7.5 pM Alexa647-labeled) was added prior to imaging. Top: Image of N-WASP and the mask generated from Otsu thresholding. Bottom: Arp2/3 complex images. Red lines indicate mask. Green arrow indicates a molecule localized outside of clusters. Scale bar = 5 μm. **(E)** Histogram of Arp2/3 complex dwell times for molecules localized inside and outside of clusters. Data from 15,042 tracks of molecules inside clusters and 24,398 tracks of molecules outside clusters. The Y-axis is set to display all bins containing at least 3 tracks. **(F)** Percent of long-lived Arp2/3 complexes (dwell time > 3 s) inside clusters across a range of Nephrin/Nck/N-WASP stoichiometries. Data from multiple experiments were compiled to determine the cumulative distribution from at least 1,000 tracks per condition. Red dotted line represents the percent long lived Arp2/3 complexes outside clusters (6%). Details about number of measurements are in Table S3 **(G)** Percent of long lived Arp2/3 complexes versus N-WASP membrane dwell time (data from C and F). Black diagonal line shows a linear fit of the data (Pearson r = 0.63, $p<0.01$). **(H)** Representative image of N-WASP-mEmearld in a U2OS cell expressing Nephrin-BFP, N-WASP-mEmerald and Nck-mCherry. Timelapse images of clusters in the region highlighted by the red box. Scale bar = 10 μm. **(I)** Representative quantification of FRAP analysis of the cluster indicated by the yellow circle. **(J)** N-WASP FRAP tau versus Nck intensity in clusters. Data collected from over 20 cells in four independent experiments. Each point represents the mean +/− SEM. Details about number of measurements are in Table S4.

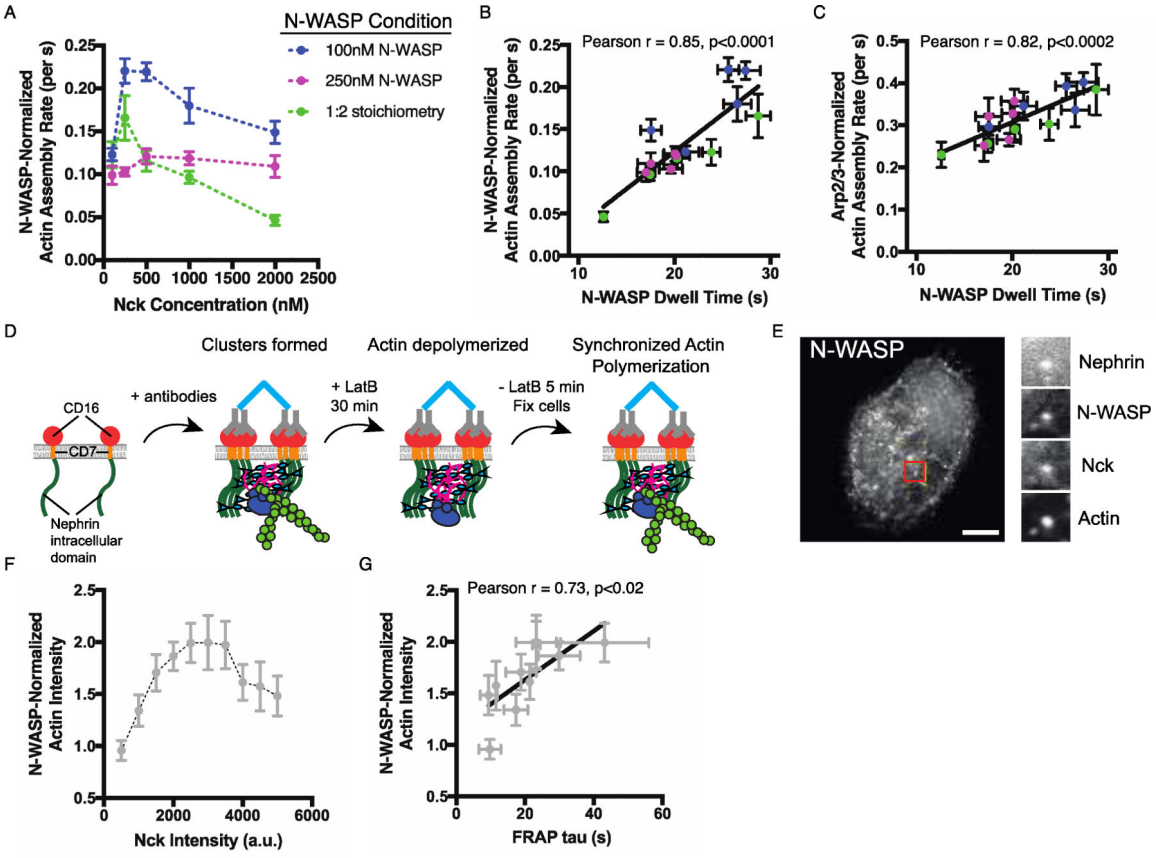

Fig. 4.

Stoichiometry of pNephrin, Nck and N-WASP regulates N-WASP and Arp2/3 complex activity in phase separated membrane clusters.

(A) N-WASP-normalized actin assembly rate in clusters formed by adding N-WASP (15% Alexa488 labeled) and Nck at the indicated concentrations to membrane-bound pNephrin (~1000 molecules/μm^2). Each point represents the mean +/− SEM from at least 13 measurements. Details about number of measurements are in Table S5. **(B)** N-WASP-normalized actin assembly rate versus N-WASP membrane dwell time (data from Figs. 3c and 4a). Black diagonal line represents a linear fit of the data (Pearson r = 0.85, p<0.0001). **(C)** Arp2/3-normalized actin assembly rate versus N-WASP membrane dwell time (data from Figs. 3c and 4a). Black diagonal line represents a linear fit of the data (Pearson r = 0.82, p<0.0002). Note that data in Figure 4 are not quantitatively comparable to those in Figures 2e–f and S6c–d, as different buffer and actin concentrations were used in the different experiments. Both datasets are, however, internally comparable. **(D)** Schematic of cellular actin assembly assay. Molecules not drawn to scale. **(E)** LEFT: Representative image of N-WASP-mEmerald in a U2OS cell expressing Nephrin-BFP, N-WASP-mEmerald, Nck-mCherry, and stained with phalloidin-Alexa 647 to label actin filaments. RIGHT: Images of all four labeled molecules colocalized in a single cluster in the region highlighted by a red box. Scale bar = 10 μm. **(F)** N-WASP-normalized actin intensity versus Nck intensity in clusters containing similar intensities of Nephrin-BFP and N-WASP-mEmerald. Data collected from over 20 cells in three independent experiments. Each point represents

the mean +/− SEM from measurements in at least 2 cells. Details about number of measurements are in Table S6. **(G)** N-WASP-normalized actin intensity versus N-WASP FRAP tau (Data from Figs 3j and 4f). Black diagonal line represents a linear fit of the data (Pearson $r = 0.73$, $p<0.02$).